

1 **TITLE:** Mice infected with *Mycobacterium tuberculosis* are resistant to secondary
2 infection with SARS-CoV-2

3

4 **RUNNING TITLE:** *M. tuberculosis* and SARS-CoV-2 coinfection in mice

5

6 **AUTHORS:** Oscar Rosas Mejia ¹, Erin S. Gloag ¹, Jianying Li ², Marisa Ruane-Foster ¹,
7 Tiffany A. Claeys ¹, Daniela Farkas ³, Laszlo Farkas ³, Gang Xin ^{1,2}, Richard T. Robinson

8 ^{1,*}

9

10 **AFFILIATIONS:** ¹ Department of Microbial Infection and Immunity; ² Pelotonia Institute
11 for Immuno-Oncology; ³ Department of Internal Medicine, Division of Pulmonary, Critical
12 Care and Sleep Medicine, Davis Heart and Lung Research Institute, The Ohio State
13 University, Columbus, OH, USA.

14

15 * Corresponding author

16 **ABSTRACT**

17 *Mycobacterium tuberculosis* (Mtb) and SARS-CoV-2 (CoV2) are the leading causes of
18 death due to infectious disease. Although Mtb and CoV2 both cause serious and
19 sometimes fatal respiratory infections, the effect of Mtb infection and its associated
20 immune response on secondary infection with CoV2 is unknown. To address this question
21 we applied two mouse models of COVID19, using mice which were chronically infected
22 with Mtb. In both model systems, Mtb-infected mice were resistant to secondary CoV2
23 infection and its pathological consequences, and CoV2 infection did not affect Mtb
24 burdens. Single cell RNA sequencing of coinfecte^d and monoinfected lungs
25 demonstrated the resistance of Mtb-infected mice is associated with expansion of T and
26 B cell subsets upon viral challenge. Collectively, these data demonstrate that Mtb
27 infection conditions the lung environment in a manner that is not conducive to CoV2
28 survival.

29

30 **AUTHOR SUMMARY**

31 *Mycobacterium tuberculosis* (Mtb) and SARS-CoV-2 (CoV2) are distinct organisms which
32 both cause lung disease. We report the surprising observation that Mtb-infected mice are
33 resistant to secondary infection with CoV2, with no impact on Mtb burden and resistance
34 associating with lung T and B cell expansion.

35 INTRODUCTION

36 The world is currently in the midst of two lung disease pandemics: COVID19 and
37 tuberculosis (TB), the causative agents of which are SARS-CoV-2 (CoV2) and
38 *Mycobacterium tuberculosis* (Mtb), respectively. Although COVID19 and TB both pose
39 enormous health challenges, especially in countries where COVID19 vaccines are
40 scarce, it is unknown what effect Mtb infection has on host responses to CoV2 as
41 there are few clinical reports of Mtb/CoV2 coinfection in the absence of other
42 comorbidities [1, 2]. On the one hand, CoV2 infection may exacerbate the inflammatory
43 response and pulmonary complications experienced by individuals with TB [3], analogous
44 to that which is observed in the Mtb/Influenza A or Mtb/CMV coinfecting individuals [4-7].
45 On the other hand, there is an inverse relationship between TB incidence rates and
46 COVID19 mortality in numerous countries [8], and *Mycobacterium* spp express several
47 proteins homologous to CoV2 antigens [9-11], raising the possibility that adaptive immune
48 responses to Mtb may confer heterologous immunity against CoV2. To definitively
49 address whether Mtb-infection impacts CoV2 elicited lung disease in a controlled setting,
50 we applied two mouse models of COVID19 (CoV2 infection of K18-hACE2 mice [12], and
51 mouse-adapted CoV2 [MACoV2] infection of C57BL/6 mice [13]), using mice that were
52 chronically infected with Mtb. The results below support a model wherein Mtb infection
53 confers resistance to secondary infection with CoV2 and its pathological consequences.
54 The implications of these data for our understanding of COVID19 susceptibility and the
55 limitations of our study are discussed.

56 **RESULTS**

57 Details regarding the origin, culture, preparation and authentication of CoV2 (strain USA-
58 WA1/2020), MACoV2 (strain MA10) and Mtb (strain H37Rv) are provided in our *Methods*.
59 To determine if host responses to CoV2 are affected by Mtb-infection, K18-hACE2
60 (ACE2) and C57BL/6 (B6) mice were infected with low dose Mtb (~90 CFU) via aerosol
61 delivery; thirty days later, the ACE2 mice were challenged with CoV2 (~25K PFU) via
62 intranasal delivery (**FIG 1A**). These Mtb/CoV2 co-infected (Mtb^{POS}CoV2^{POS}) ACE2 mice
63 were monitored daily for changes in weight, as were two control groups: ACE2 mice which
64 were Mtb-infected at the same time (Day -30) but challenged with sterile media
65 (Mtb^{POS}CoV2^{NEG}), and ACE2 mice which were not Mtb-infected prior to CoV2 challenge
66 (Mtb^{NEG}CoV2^{POS}). On post-challenge Days 4, 7 and 14, groups of mice were euthanized
67 and the lungs and other tissues were removed to assess Mtb and CoV2 burdens, as well
68 as a number of immunological readouts. All mice were identically housed for the duration
69 of the entire experiment. As anticipated, Mtb^{NEG}CoV2^{POS} ACE2 mice lost a significant
70 portion of body weight by post-challenge Day 7 (<20%) (**FIG 1B**). Mtb^{POS}CoV2^{POS} ACE2
71 mice, however, did not lose significant body weight and were otherwise indistinguishable
72 from Mtb^{POS}CoV2^{NEG} controls (**FIG 1B**). On post-challenge Day 4, lung CoV2 burdens
73 were lower in Mtb^{POS}CoV2^{POS} mice relative to Mtb^{NEG}CoV2^{POS} mice, as assessed by
74 either plaque assay (**FIG 1C**) or CoV2 N protein measurement (**FIG 1D**). Challenge with
75 CoV2 did not affect Mtb growth, as Mtb CFU burdens in Mtb^{POS}CoV2^{POS} and
76 Mtb^{POS}CoV2^{NEG} lungs did not differ after challenge (**FIG 1E**), nor did they differ in spleen
77 (**FIG 1F**) or liver (**FIG 1G**). Consistent with the above Mtb CFU results, the abundance of
78 acid fast bacilli (AFB) was also similar between Mtb^{POS}CoV2^{POS} and Mtb^{POS}CoV2^{NEG}

79 lungs (**FIG 1H**). Transgenic human ACE2 expression also does affect Mtb growth, as
80 CFU burdens in Mtb^{POS}CoV2^{NEG} ACE2 mice were indistinguishable from Mtb-infected B6
81 controls (**FIG 1E-G**).

82

83 We next assessed the impact of Mtb infection on CoV2-elicited immune responses in the
84 lung, using tissue from the same ACE2 transgenic mice described above. CoV2 infection
85 elicits the expression of multiple inflammatory genes in mouse lungs [12]. Consistent with
86 this, protein levels of IFN γ , IL6 and IL1 β were elevated in Mtb^{NEG}CoV2^{POS} lungs post-
87 challenge Day 4 and/or Day 7, relative to uninfected (UI) controls (**FIG 2A-C**). In
88 Mtb^{POS}CoV2^{NEG} mice, lung protein levels of IFN γ , IL6 and IL1 β were even higher, and
89 were not affected by CoV2 challenge (**FIG 2A-C**, compare Mtb^{POS}CoV2^{NEG} and
90 Mtb^{POS}CoV2^{POS} levels). This pattern, wherein Mtb monoinfection induces high levels of
91 a gene expression that are unchanged upon CoV2 challenge, was also observed for IFN γ
92 and TNF α at the mRNA level (**FIG 2D-E**); however and notably, the resistance of
93 Mtb^{POS}CoV2^{POS} mice did not associate with elevated expression of the antiviral genes
94 IFIT2 and IFIT3, which are otherwise induced in Mtb^{NEG}CoV2^{POS} mice (**FIG 2F-G**), nor
95 was CoV2 able to induce CCL2 expression in the presence of Mtb (**FIG 2H**). Expression
96 of the anti-inflammatory cytokine IL10 was low in all experimental groups related to UI
97 controls (**FIG 2I**).

98

99 At a histological level, the lungs of Mtb^{NEG}CoV2^{POS} mice exhibited a number of previously
100 reported features [14] by post-challenge Day 4 (**FIG 3A**) and Day 7 (**FIG 3B**), including
101 diffuse alveolar damage with inflammatory infiltrates and alveolar necrosis. Since these

102 features were also observed in granulomatous lesions of $Mtb^{POS}CoV2^{NEG}$ lungs, a
103 hallmark of Mtb infection, we could not use histology to observe whether Mtb inhibits
104 $CoV2$ -induced inflammation and alveolar necrosis. What could be observed, however,
105 were differences between $Mtb^{NEG}CoV2^{POS}$ and $Mtb^{POS}CoV2^{POS}$ lungs with regards to
106 hyaline membrane formation and pneumonia in the terminal bronchioles by Day 7 (**FIG**
107 **3B inset**), which were notable in $Mtb^{NEG}CoV2^{POS}$ lungs but absent from $Mtb^{POS}CoV2^{POS}$
108 lungs (pneumonia is not typical of Mtb -infected mice on the B6 background until ~1 year
109 after infection [15]). Consistent with our assessment of lung $CoV2$ burdens (**FIG 1C-D**),
110 anti-N protein immunohistochemistry (IHC) staining demonstrated fewer and less intense
111 IHC+ regions within $Mtb^{POS}CoV2^{POS}$ lungs, relative to $Mtb^{NEG}CoV2^{POS}$ lungs (**FIG 3C-D**).
112 Notably, the few IHC+ regions which were observed in $Mtb^{POS}CoV2^{POS}$ lungs were distal
113 to granulomatous lesions that contain Mtb (**FIG 3C**).
114

115 To determine whether Mtb -induced resistance to $CoV2$ was specific to the ACE2
116 transgenic model of COVID19, we performed the same set of experiments using a second
117 mouse model of COVID19: MACoV2 infection of B6 mice [13]. As before, our
118 experimental groups included B6 mice which were uninfected prior to MACoV2 challenge
119 ($Mtb^{NEG}MACoV2^{POS}$), or Mtb -infected 30 days prior to challenge with MACoV2
120 ($Mtb^{POS}MACoV2^{POS}$) or vehicle control ($Mtb^{POS}MACoV2^{NEG}$) (**FIG 4A**). Whereas ACE2
121 mice which lost $\leq 20\%$ body weight within 7 days of $CoV2$ challenge (**FIG 1B**), MACoV2
122 induced weight loss was less dramatic, with $Mtb^{NEG}MACoV2^{POS}$ mice losing $\leq 10\%$ body
123 weight within 7 days of MACoV2 challenge (**FIG 4B**). Nevertheless and consistent with
124 our ACE2 model results, $Mtb^{POS}MACoV2^{POS}$ were resistant to MACoV2-elicited weight

125 loss (**FIG 4B**), had lower viral burdens compared to $Mtb^{NEG}MACoV2^{POS}$ mice (**FIG 4C-D**)
126 and no change in lung Mtb burdens following virus challenge (**FIG 4E**). Following virus
127 challenge, $Mtb^{NEG}MACoV2^{POS}$ lungs exhibited transient increases in protein and mRNA
128 levels of $IFN\gamma$ (**FIG 4F-G**), $IL6$ (**FIG 4H**), $IFIT3$ (**FIG 4I**), $IFITM3$ (**FIG 4J**) and $ACE2$ (**FIG**
129 **4K**), consistent with previous reports of CoV2 inducing expression of its own receptor
130 [16]. As was also observed in the $ACE2$ model (**FIG 2A-B**), protein levels of $IFN\gamma$ and $IL6$
131 were already high in $Mtb^{POS}MACoV2^{NEG}$ lungs and unaffected by MACoV2 challenge (**FIG**
132 **4F, H**). MACoV2 elicited $IFIT3$ expression in both $Mtb^{NEG}MACoV2^{POS}$ and
133 $Mtb^{POS}MACoV2^{POS}$ lungs, albeit lower in the latter group (**FIG 4J**). The resistance of Mtb -
134 infected B6 mice to CoV2 was not attributable to an absence of lung $ACE2$ expression,
135 as $Mtb^{POS}MACoV2^{POS}$ mice expressed higher than UI levels of $ACE2$ (**FIG 4K**); unlike
136 $Mtb^{NEG}MACoV2^{POS}$ mice, however, $ACE2$ expression in $Mtb^{POS}MACoV2^{POS}$ lungs was
137 not affected by MACoV2 challenge (**FIG 4K**).

138
139 Finally, to discern the lung immune environment associated with MACoV2 resistance in
140 Mtb -infected mice, we used scRNA-seq to analyze live $CD45^+$ cells from the lungs of
141 each group (UI, $Mtb^{NEG}MACoV2^{POS}$, $Mtb^{POS}MACoV2^{NEG}$ and $Mtb^{POS}MACoV2^{POS}$) on
142 post-challenge Day 7. This timepoint enabled us to analyze immune cells after PFU are
143 no longer detectable (**FIG 4C**). Live $CD45^+$ cells were purified from the lungs of each
144 group (4 mice per group) and used to prepare single-cell transcriptome datasets. These
145 datasets separated into 12 clusters using the dimensionality reduction and clustering
146 algorithms in the 10X Cell Ranger pipeline (**FIG 5A-C**). The expression profile of 20
147 myeloid and lymphoid lineage markers (*S100a4*, *S100a9*, *Cd8b1*, *Cd4*, *Cd79a*, *Ms4a1*,

148 *Cybb, Mafb, Cd3g, Fcgr3, Cst3, Nme1, Itgam, Cd8a, Lig1, Ccna2, Ccr7, Il7r, Ncr1* and
149 *Nkg7*) allowed us to assign biological identities to each cluster (**FIG 5D**). For each lineage
150 marker, the average expression and percent positivity within each cluster were similar
151 across all experimental groups (**SFIG1**). We identified four T cell clusters (clusters 0, 2, 4
152 and 7), two B cell clusters (clusters 3 and 9), three myeloid-cell clusters (clusters 6, 8,
153 and 10), one basophil cluster (cluster 11), one neutrophil cluster (cluster 5), and one
154 natural killer–cell cluster (cluster 1) (**FIG 5A**). The extent to which these clusters were
155 represented among all CD45+ cells varied by group (**FIG 5C, E**). We observed that innate
156 clusters (i.e. NK, neutrophil, DC, MØ, CD11b+ MØ and basophils) comprised 50% of the
157 UI lung, with T cells (42 %) and B cells (8%) making up the difference (**FIG 5D**). In
158 $Mtb^{NEG}MACoV2^{POS}$ lungs, the representation of T cell (51 %) and B cell (16 %) clusters
159 was higher, as were DC (4 %) and MØ (7 %) clusters. Relative to UI lungs, the
160 $Mtb^{POS}MACoV2^{NEG}$ lung was characterized by the expansion of nearly all immune
161 clusters (CD8 T cells, 8→15%; B cells, 6→13%; CD8 memory T cells, 7→9%; DCs,
162 2→4%; CD4 T cells, 3→6%; CD11b+ MØ, 1→2%; activated B cells, 2→4%; MØ, 1→5%)
163 at the expense of neutrophils (17→7%), NK cells (28→15%) and naïve T cells (24→21%).
164 Importantly, the profile of $Mtb^{POS}MACoV2^{POS}$ lungs closely resembled that of
165 $Mtb^{POS}MACoV2^{NEG}$ lung, with the exception of expanded B cell (17%), CD8 memory T
166 cell (10%), DC (6%) and activated B cell (5%) clusters, again at the expense of
167 neutrophils, NK cells and naïve T cells (**FIG 5D**). Collectively, our scRNA seq data
168 demonstrates the resistance of *Mtb*-infected mice to MACoV2 is associated with a lung
169 immune environment that is largely similar to that observed in *Mtb* monoinfected lungs,
170 with the exception of expanded T and B cell clusters.

171 **DISCUSSION**

172 Our results demonstrate that Mtb infected mice are resistant to secondary infection with
173 CoV2 and its pathological consequences. With regards to the mechanism of resistance,
174 we believe the inflammatory nature of Mtb infection creates a lung environment that is
175 inhospitable to CoV2 propagation. In the absence of Mtb, CoV2 enter cells via ACE2,
176 propagates and triggers an inflammatory response that extends after CoV2 clearance
177 and causes declines in lung function and death. In the presence of Mtb, CoV2 entry is
178 likely unaffected since ACE2 is abundantly expressed in the Mtb-infected lung, but the
179 extent of CoV2 propagation is low and the immunopathological responses typically
180 triggered in mice (i.e. weight loss, pneumonia) are muted. This is likely due to one or both
181 of the following reasons: (1) Mtb infected lungs already contain an array of immune innate
182 lineages which restrict CoV2, or (2) Mtb elicits an adaptive immune response that cross
183 reacts with CoV2 antigens and offers heterologous immunity. This latter explanation is
184 supported by recent epidemiological studies of COVID among individuals vaccinated with
185 *M. bovis* BCG [17-19], which depending on the strain has significant antigenic overlap
186 with Mtb [20, 21]. The limitations of our study include its being performed in mice, which
187 of course do not recapitulate all aspects of TB or COVID in humans, nor have we
188 examined the long term impact of CoV2 on the host response to Mtb as we terminated
189 our study fourteen days after CoV2 challenge. That said, we believe animal models of
190 TB and COVID are ideal for studies of this nature because—if studies of COVID in
191 individuals with other chronic lung diseases are any guide [22, 23]—it will likely be difficult
192 to tease apart the impact of TB on COVID outcomes in humans given that individuals with
193 TB often have numerous other comorbidities (e.g. malnourishment, HIV) that confound

194 interpretation. Translated to human COVID susceptibility, our results suggest that
195 individuals infected with Mtb generate an immune response that offers a degree of
196 protection from subsequent or secondary infection with CoV2.

197 **MATERIALS & METHODS**

198

199 **SARS-CoV-2 culture, preparation and authentication.** All experiments involving
200 SARS-CoV-2 followed procedures and protocols that are approved by The Ohio State
201 University (OSU) Institutional Biosafety Committee. SARS-CoV-2, isolate USA-
202 WA1/2020, was obtained from Biodefense and Emerging Infections Research Resources
203 Repository (BEI Resources, Batch # 70034262). Mouse adapted SARS-CoV-2 variant
204 strain MA10 [24] was likewise provided by BEI Resources (Cat # NR-55329). Virus was
205 cultured, prepared and authenticated as we recently reported [25]. Namely, to establish
206 the viral stocks used in our studies, a virus aliquot was thawed, diluted 1:10,000 in
207 incomplete DMEM (Gibco; supplemented with 4.5 g/L D-glucose, 110 mg/L sodium
208 pyruvate) and added to confluent VeroE6 cells (ATCC). Cells were incubated with virus
209 for 1h (37°C, 5% CO₂), after which time the media was replaced with complete DMEM
210 (i.e. DMEM prepared as above, further supplemented with 4% heat-inactivated fetal
211 bovine serum) and the cells were incubated for 3 days (37°C, 5% CO₂) to allow virus
212 propagation. After that period, visual inspection under light microscopy demonstrated
213 near complete death of the infected VeroE6 cells. The supernatant was collected into
214 50mL conicals, centrifuged at low speed to remove cell debris and subsequently
215 aliquoted, frozen and stored at -80°C. These frozen aliquots served as the stock tubes
216 for all subsequent experiments. The live virus titer of our frozen aliquots was determined
217 via the plaque assay described below. SARS-CoV-2 stocks were authenticated using a
218 clinically validated clinical next-generation sequencing assay [26].

219 ***Mycobacterium tuberculosis* culture, preparation and authentication.** All
220 experiments involving *M. tuberculosis* (Mtb) followed procedures and protocols that are
221 approved by The Ohio State University (OSU) Institutional Biosafety Committee. The
222 virulent Mtb strain H37Rv (Trudeau Institute, Saranac Lake, NY) was grown in Proskauer
223 Beck medium containing 0.05% tyloxapol to mid-log phase (37°C, 5% CO₂) and frozen in
224 1-ml aliquots at -80°C. The live bacteria titer of our frozen aliquots was determined via
225 plating serial dilutions on 7H11 agar media. To authenticate our Mtb stock we confirmed
226 that the colony morphology, *in vitro* growth characteristics and *in vivo* virulence were
227 consistent with our previous studies using the H37Rv strain [27].

228

229 **Mice.** All mice were treated in accordance with OSU Institutional Animal Care and Use
230 Committee (IACUC) guidelines and approved protocols. C57BL/6 and hemizygous K18-
231 hACE C57BL/6J mice (strain: 2B6.Cg-Tg(K18-ACE2)2PrImn/J) were purchased from
232 Jackson Laboratory (Bar Harbor, ME) and housed at OSU within an AALAC-accredited
233 facility (University Laboratory Animal Resources, ULAR).

234

235 **Aerosol Mtb infection.** Mice were aerosol infected with Mtb H37Rv per our previous
236 studies using the Glas-Col inhalation system [27]. For bacterial load determinations, the
237 lungs, spleen, and liver were aseptically removed and individually homogenized in sterile
238 normal saline (Gentle Macs system, program “RNA” run 2X). Serial dilutions of each
239 organ were then plated on 7H11 and colonies counted after 2-3 weeks incubation at 37°C
240 5% CO₂. Lungs from control mice were plated on post-infection Day 1 to verify the delivery
241 of ~80 Mtb CFU.

242

243 **Intranasal CoV2 challenge.** Mice that were either uninfected (UI) or previously infected
244 with aerosol Mtb (Mtb^{POS}) mice were challenged with either CoV2 or MACoV2. At the time
245 of challenge, mice were anesthetized with isoflurane, weighed and held at a semi-supine
246 position while 50 μ L of CoV2-containing PBS (2.5×10^4 PFU) or MACoV2 (2.5×10^4 PFU)
247 was given via intranasal (i.n.) instillation. Control mice were given the same volume of
248 sterile PBS, using the same anesthesia and i.n. instillation protocol. After i.n. instillation,
249 each mouse was returned to its home cage, house and monitored daily for changes in
250 weight or body condition. For viral load determinations, the lungs of challenged animals
251 were aseptically removed and individually homogenized as described above; serial
252 dilutions were then used in the plaque assay described below.

253

254 **CoV2 plaque assay.** A modified version of the plaque assay developed by the Diamond
255 laboratory [28] was used to determine lung viral burdens in challenged animals, the
256 details of which we have reported [29]. Namely, one day prior to the assay start we
257 seeded 12-well with VeroE6 cells and incubated overnight (37°C 5% CO₂) such that each
258 well was confluent by the assay start. On the day of the assay, serial dilutions of virus-
259 containing material (e.g. lung homogenate) were prepared in cDMEM and warmed to
260 37°C . Media from each well of the 12-well plate was gently removed via pipette and
261 replaced with 500uL of each virus sample dilution, the volume pipetted down the side of
262 the well so as not to disturb the VeroE6 monolayer. The plate was incubated for 1 hr at
263 37°C 5% CO₂. During this incubation period, a solution comprising a 1:0.7 mixture of
264 cDMEM and 2% methylcellulose (viscosity: 4000 cP) was freshly made and warmed to

265 37°C in a water bath. After the 1 hr incubation period was over, the supernatant was
266 removed from each well and replaced with 1 mL of the pre-warmed
267 cDMEM:methylcellulose mixture. The culture plate was then returned to the incubator and
268 left undisturbed for 3 days. On the final day, the cDMEM:methylcellulose mixture was
269 removed from each well, cells were fixed with 4% para-formaldehyde in PBS (20 minutes,
270 room temperature), washed with PBS and stained with 0.05% crystal violet (in 20%
271 methanol). After rinsing plates with distilled water, plates were dried, and plaques were
272 counted under a light microscope.

273

274 **Histology.** The inferior lung lobe was removed from mice and fixed in 10% formalin.
275 Sample processing, paraffin embedding, H&E and acid fast bacilli (AFB) staining was
276 performed by the OSU Comparative Pathology & Mouse Phenotyping Shared Resource
277 (CPMPSR). Immunohistochemistry (IHC) was performed using a monoclonal antibody
278 specific to SARS-CoV-2 Nucleocapsid (clone B46F; ThermoFisher) per previously
279 reported methods [30]. Histology slides were imaged using a Nikon Ti2 widefield
280 microscope fitted with 4x, 10x and 60x CFI Plan Fluor objectives and a DS-Fi3 color
281 camera. Images were processed using FIJI [31] and compiled using BioRender.com

282

283 **ELISA.** CoV2 N protein levels in lung homogenates were determined using a
284 commercially available ELISA kit (ADS Biotec), as were protein levels of the cytokines
285 IL1 β , IL6 and IFN γ (Biolegend). ELISA kits were used per manufacturer protocols.

286

287 **Quantitative Real Time PCR.** Lung RNA was extracted from the superior lung lobe using
288 the RNeasy Mini Kit method (Qiagen) and reverse transcribed using the SuperScript VILO
289 cDNA Synthesis Kit method (ThermoFisher). Quantitative real time PCR (qRT-PCR) was
290 performed on a C1000 Touch Thermocycler (Bio-Rad) using SYBR Select Master Mix
291 (Applied Biosystems) per manufacturer protocols. The primer sequences used to amplify
292 cDNA for genes of interest were previously published [32, 33]. Each biological replicate
293 was performed in technical duplicate and data were analyzed using the $\Delta\Delta Ct$ method.

294

295 **Cell purification.** To purify live CD45+ cells for single cell RNA sequencing, lungs from
296 uninfected, Mtb- or MACoV2-monoinfected and Mtb/MACoV2 coinfecte mice were
297 removed and treated in an identical manner. Lungs were first digested in a
298 DNase/collagenase mixture [34]; dead cells from the resulting slurry were then removed
299 via negative magnetic selection using the Dead Cell Removal kit method (Miltenyi). The
300 live cells were then mixed with CD45 microbeads (Miltenyi) and used for positive
301 magnetic selection of live CD45+ cells. Trypan blue staining was used to confirm cell
302 viability. Cells were the prepared for single cell partitioning via a 10X Genomics Chromium
303 Controller using manufacturer provided protocols (10x Genomics Document Number
304 CG000136). 1×10^4 cells per experimental group were loaded onto the Controller and
305 partitioned, as carried out by the OSU Genomics Shared Resource core.

306

307 **Single cell RNA sequencing (scRNA seq).** scRNA-seq libraries were prepared and
308 analyzed using the 10X Genomics and Illumina platforms, respectively, per previously
309 reported methods [35].

310

311 **Statistical analysis.** All experiments were performed using randomly assigned mice
312 without investigator blinding. All data points and *p* values reflect biological replicates from
313 at least two independent experiments per figure (4 mice per group per timepoint).
314 Statistical analysis was performed using GraphPad Prism. Unpaired, two-tailed Student t
315 tests and one-way ANOVA tests with post hoc Tukey-Kramer corrections were used to
316 assess statistical significance. Graphs were likewise generated in GraphPad Prism. The
317 only exception to this were the t-distributed stochastic neighbor embedding (t-SNE),
318 annotation and graphing associated with our scRNA analysis, which was performed with
319 Cell Ranger and RStudio.

320 **ACKNOWLEDGEMENTS**

321 The project described was supported by funds from the NIH/NIAID (R01AI121212 to
322 RTR) and The Ohio State University (OSU). ORM was funded by an OSU Advancing
323 Research in Infection and Immunity Fellowship Award; ESG was funded by an American
324 Heart Association Career Development Award (19CDA34630005). We would like to
325 acknowledge the laboratories of Jianrong Li (OSU), Mark Peeples (OSU & Nationwide
326 Children's Hospital) and Jacob Yount (OSU) who grew and provided the MCoV2 used
327 in our studies, as well as BSL3 Director Luanne Hall-Stoodley and BSL3 Research
328 Assistant Abigail Mayer for maintaining the facilities needed for our studies.

329 REFERENCES

330

331 1. Riou C, du Bruyn E, Stek C, Daroowala R, Goliath RT, Abrahams F, et al.
332 Relationship of SARS-CoV-2-specific CD4 response to COVID-19 severity and impact of
333 HIV-1 and tuberculosis coinfection. *J Clin Invest.* 2021;131(12). Epub 2021/05/05. doi:
334 10.1172/JCI149125. PubMed PMID: 33945513; PubMed Central PMCID:
335 PMC8203446.

336 2. Tamuzi JL, Ayele BT, Shumba CS, Adetokunboh OO, Uwimana-Nicol J, Haile ZT,
337 et al. Implications of COVID-19 in high burden countries for HIV/TB: A systematic review
338 of evidence. *BMC Infect Dis.* 2020;20(1):744. Epub 2020/10/11. doi: 10.1186/s12879-
339 020-05450-4. PubMed PMID: 33036570; PubMed Central PMCID: PMC7545798.

340 3. Mousquer GT, Peres A, Fiegenbaum M. Pathology of TB/COVID-19 Co-Infection:
341 The phantom menace. *Tuberculosis (Edinb).* 2021;126:102020. Epub 2020/11/28. doi:
342 10.1016/j.tube.2020.102020. PubMed PMID: 33246269; PubMed Central PMCID:
343 PMC7669479.

344 4. MENDY J, Jarju S, Heslop R, Bojang AL, Kampmann B, Sutherland JS. Changes in
345 Mycobacterium tuberculosis-Specific Immunity With Influenza co-infection at Time of TB
346 Diagnosis. *Front Immunol.* 2018;9:3093. Epub 2019/01/22. doi:
347 10.3389/fimmu.2018.03093. PubMed PMID: 30662443; PubMed Central PMCID:
348 PMC6328457.

349 5. Cobelens F, Nagelkerke N, Fletcher H. The convergent epidemiology of
350 tuberculosis and human cytomegalovirus infection. *F1000Res.* 2018;7:280. Epub
351 2018/05/24. doi: 10.12688/f1000research.14184.2. PubMed PMID: 29780582; PubMed
352 Central PMCID: PMC5934687.

353 6. Walaza S, Tempia S, Dawood H, Variava E, Moyes J, Cohen AL, et al. Influenza
354 virus infection is associated with increased risk of death amongst patients hospitalized
355 with confirmed pulmonary tuberculosis in South Africa, 2010-2011. *BMC Infect Dis.*
356 2015;15:26. Epub 2015/01/28. doi: 10.1186/s12879-015-0746-x. PubMed PMID:
357 25623944; PubMed Central PMCID: PMC4316613.

358 7. Redford PS, Mayer-Barber KD, McNab FW, Stavropoulos E, Wack A, Sher A, et
359 al. Influenza A virus impairs control of Mycobacterium tuberculosis coinfection through a
360 type I interferon receptor-dependent pathway. *J Infect Dis.* 2014;209(2):270-4. Epub
361 2013/08/13. doi: 10.1093/infdis/jit424. PubMed PMID: 23935205; PubMed Central
362 PMCID: PMC3873785.

363 8. Inoue K, Kashima S. Association of the past epidemic of Mycobacterium
364 tuberculosis with mortality and incidence of COVID-19. *PLoS One.* 2021;16(6):e0253169.
365 Epub 2021/06/19. doi: 10.1371/journal.pone.0253169. PubMed PMID: 34143810;
366 PubMed Central PMCID: PMC8213125.

367 9. Eggenhuizen PJ, Ng BH, Chang J, Fell AL, Cheong RMY, Wong WY, et al. BCG
368 Vaccine Derived Peptides Induce SARS-CoV-2 T Cell Cross-Reactivity. *Front Immunol.*
369 2021;12:692729. Epub 2021/08/24. doi: 10.3389/fimmu.2021.692729. PubMed PMID:
370 34421902; PubMed Central PMCID: PMC8374943.

371 10. Dakal TC. Antigenic sites in SARS-CoV-2 spike RBD show molecular similarity
372 with pathogenic antigenic determinants and harbors peptides for vaccine development.
373 *Immunobiology.* 2021;226(5):152091. Epub 2021/07/26. doi:

374 10.1016/j.imbio.2021.152091. PubMed PMID: 34303920; PubMed Central PMCID:
375 PMCPMC8297981.

376 11. Nuovo G, Tili E, Suster D, Matys E, Hupp L, Magro C. Strong homology between
377 SARS-CoV-2 envelope protein and a *Mycobacterium* sp. antigen allows rapid diagnosis
378 of Mycobacterial infections and may provide specific anti-SARS-CoV-2 immunity via the
379 BCG vaccine. *Ann Diagn Pathol.* 2020;48:151600. Epub 2020/08/18. doi:
380 10.1016/j.anndiagpath.2020.151600. PubMed PMID: 32805515; PubMed Central
381 PMCID: PMCPMC7423587.

382 12. Winkler ES, Bailey AL, Kafai NM, Nair S, McCune BT, Yu J, et al. SARS-CoV-2
383 infection of human ACE2-transgenic mice causes severe lung inflammation and impaired
384 function. *Nat Immunol.* 2020;21(11):1327-35. Epub 2020/08/26. doi: 10.1038/s41590-
385 020-0778-2. PubMed PMID: 32839612; PubMed Central PMCID: PMCPMC7578095.

386 13. Dinnon KH, 3rd, Leist SR, Schafer A, Edwards CE, Martinez DR, Montgomery SA,
387 et al. A mouse-adapted model of SARS-CoV-2 to test COVID-19 countermeasures.
388 *Nature.* 2020;586(7830):560-6. Epub 2020/08/28. doi: 10.1038/s41586-020-2708-8.
389 PubMed PMID: 32854108; PubMed Central PMCID: PMCPMC8034761.

390 14. Jiang RD, Liu MQ, Chen Y, Shan C, Zhou YW, Shen XR, et al. Pathogenesis of
391 SARS-CoV-2 in Transgenic Mice Expressing Human Angiotensin-Converting Enzyme 2.
392 *Cell.* 2020;182(1):50-8 e8. Epub 2020/06/10. doi: 10.1016/j.cell.2020.05.027. PubMed
393 PMID: 32516571; PubMed Central PMCID: PMCPMC7241398.

394 15. Rhoades ER, Frank AA, Orme IM. Progression of chronic pulmonary tuberculosis
395 in mice aerogenically infected with virulent *Mycobacterium* tuberculosis. *Tuber Lung Dis.*
396 1997;78(1):57-66. Epub 1997/01/01. doi: 10.1016/s0962-8479(97)90016-2. PubMed
397 PMID: 9666963.

398 16. Ziegler CGK, Allon SJ, Nyquist SK, Mbano IM, Miao VN, Tzouanas CN, et al.
399 SARS-CoV-2 Receptor ACE2 Is an Interferon-Stimulated Gene in Human Airway
400 Epithelial Cells and Is Detected in Specific Cell Subsets across Tissues. *Cell.*
401 2020;181(5):1016-35 e19. Epub 2020/05/16. doi: 10.1016/j.cell.2020.04.035. PubMed
402 PMID: 32413319; PubMed Central PMCID: PMCPMC7252096.

403 17. Escobar LE, Molina-Cruz A, Barillas-Mury C. BCG vaccine protection from severe
404 coronavirus disease 2019 (COVID-19). *Proc Natl Acad Sci U S A.* 2020;117(30):17720-
405 6. Epub 2020/07/11. doi: 10.1073/pnas.2008410117. PubMed PMID: 32647056; PubMed
406 Central PMCID: PMCPMC7395502.

407 18. Hauer J, Fischer U, Auer F, Borkhardt A. Regional BCG vaccination policy in
408 former East- and West Germany may impact on both severity of SARS-CoV-2 and
409 incidence of childhood leukemia. *Leukemia.* 2020;34(8):2217-9. Epub 2020/06/20. doi:
410 10.1038/s41375-020-0871-4. PubMed PMID: 32555367; PubMed Central PMCID:
411 PMCPMC7301049.

412 19. O'Neill LAJ, Netea MG. BCG-induced trained immunity: can it offer protection
413 against COVID-19? *Nat Rev Immunol.* 2020;20(6):335-7. Epub 2020/05/13. doi:
414 10.1038/s41577-020-0337-y. PubMed PMID: 32393823; PubMed Central PMCID:
415 PMCPMC7212510.

416 20. Coppola M, Jurion F, van den Eeden SJF, Tima HG, Franken K, Geluk A, et al. In-
417 vivo expressed *Mycobacterium* tuberculosis antigens recognised in three mouse strains
418 after infection and BCG vaccination. *NPJ Vaccines.* 2021;6(1):81. Epub 2021/06/05. doi:

419 10.1038/s41541-021-00343-2. PubMed PMID: 34083546; PubMed Central PMCID:
420 PMCPMC8175414.

421 21. Zhang W, Zhang Y, Zheng H, Pan Y, Liu H, Du P, et al. Genome sequencing and
422 analysis of BCG vaccine strains. *PLoS One*. 2013;8(8):e71243. Epub 2013/08/27. doi:
423 10.1371/journal.pone.0071243. PubMed PMID: 23977002; PubMed Central PMCID:
424 PMCPMC3747166.

425 22. Lacedonia D, Scioscia G, Santomaso C, Fuso P, Carpagnano GE, Portacci A, et
426 al. Impact of smoking, COPD and comorbidities on the mortality of COVID-19 patients.
427 *Sci Rep*. 2021;11(1):19251. Epub 2021/09/30. doi: 10.1038/s41598-021-98749-4.
428 PubMed PMID: 34584165; PubMed Central PMCID: PMCPMC8478875.

429 23. Hadi YB, Lakhani DA, Naqvi SFZ, Singh S, Kupec JT. Outcomes of SARS-CoV-2
430 infection in patients with pulmonary sarcoidosis: A multicenter retrospective research
431 network study. *Respir Med*. 2021;187:106538. Epub 2021/07/30. doi:
432 10.1016/j.rmed.2021.106538. PubMed PMID: 34325226; PubMed Central PMCID:
433 PMCPMC8297986.

434 24. Leist SR, Dinnon KH, 3rd, Schafer A, Tse LV, Okuda K, Hou YJ, et al. A Mouse-
435 Adapted SARS-CoV-2 Induces Acute Lung Injury and Mortality in Standard Laboratory
436 Mice. *Cell*. 2020;183(4):1070-85 e12. Epub 2020/10/09. doi: 10.1016/j.cell.2020.09.050.
437 PubMed PMID: 33031744; PubMed Central PMCID: PMCPMC7510428.

438 25. Bednash JS, Kagan VE, Englert JA, Farkas D, Tyurina YY, Tyurin VA, et al. Syrian
439 hamsters as a model of lung injury with SARS-CoV-2 infection: pathologic, physiologic
440 and detailed molecular profiling. *Transl Res*. 2021. Epub 2021/11/07. doi:
441 10.1016/j.trsl.2021.10.007. PubMed PMID: 34740873.

442 26. Wang H, Jean S, Eltringham R, Madison J, Snyder P, Tu H, et al. Mutation-Specific
443 SARS-CoV-2 PCR Screen: Rapid and Accurate Detection of Variants of Concern and the
444 Identification of a Newly Emerging Variant with Spike L452R Mutation. *J Clin Microbiol*.
445 2021;59(8):e0092621. Epub 2021/05/21. doi: 10.1128/JCM.00926-21. PubMed PMID:
446 34011523; PubMed Central PMCID: PMCPMC8288299.

447 27. Miller HE, Robinson RT. Early control of *Mycobacterium tuberculosis* infection
448 requires *il12rb1* expression by *rag1*-dependent lineages. *Infect Immun*.
449 2012;80(11):3828-41. Epub 2012/08/22. doi: 10.1128/IAI.00426-12. PubMed PMID:
450 22907814; PubMed Central PMCID: PMCPMC3486065.

451 28. Case JB, Bailey AL, Kim AS, Chen RE, Diamond MS. Growth, detection,
452 quantification, and inactivation of SARS-CoV-2. *Virology*. 2020;548:39-48. Epub
453 2020/08/26. doi: 10.1016/j.virol.2020.05.015. PubMed PMID: 32838945; PubMed Central
454 PMCID: PMCPMC7293183.

455 29. Robinson RT, Mahfooz N, Rosas Mejia O, Liu Y, Hull NM. SARS-CoV-2
456 disinfection in aqueous solution by UV222 from a krypton chlorine excilamp. *medRxiv*.
457 2021;<https://doi.org/10.1101/2021.02.19.21252101> (Preprint posted February 23, 2021).

458 30. Farkas L, Farkas D, Ask K, Moller A, Gauldie J, Margetts P, et al. VEGF
459 ameliorates pulmonary hypertension through inhibition of endothelial apoptosis in
460 experimental lung fibrosis in rats. *J Clin Invest*. 2009;119(5):1298-311. Epub 2009/04/22.
461 doi: 10.1172/JCI36136. PubMed PMID: 19381013; PubMed Central PMCID:
462 PMCPMC2673845.

463 31. Schindelin J, Arganda-Carreras I, Frise E, Kaynig V, Longair M, Pietzsch T, et al.
464 Fiji: an open-source platform for biological-image analysis. *Nat Methods*. 2012;9(7):676-

465 82. Epub 2012/06/30. doi: 10.1038/nmeth.2019. PubMed PMID: 22743772; PubMed
466 Central PMCID: PMCPMC3855844.

467 32. Ma D, Chen CB, Jhanji V, Xu C, Yuan XL, Liang JJ, et al. Expression of SARS-
468 CoV-2 receptor ACE2 and TMPRSS2 in human primary conjunctival and pterygium cell
469 lines and in mouse cornea. *Eye (Lond)*. 2020;34(7):1212-9. Epub 2020/05/10. doi:
470 10.1038/s41433-020-0939-4. PubMed PMID: 32382146; PubMed Central PMCID:
471 PMCPMC7205026.

472 33. Lafuse WP, Rajaram MVS, Wu Q, Moliva JI, Torrelles JB, Turner J, et al. Identification of an Increased Alveolar Macrophage Subpopulation in Old Mice That
473 Displays Unique Inflammatory Characteristics and Is Permissive to *Mycobacterium*
474 tuberculosis Infection. *J Immunol*. 2019;203(8):2252-64. Epub 2019/09/13. doi:
475 10.4049/jimmunol.1900495. PubMed PMID: 31511357; PubMed Central PMCID:
476 PMCPMC6783358.

477 34. Jungblut M, Oeltze K, Zehnter I, Hasselmann D, Bosio A. Standardized preparation
478 of single-cell suspensions from mouse lung tissue using the gentleMACS Dissociator. *J
479 Vis Exp*. 2009;(29). Epub 2009/07/04. doi: 10.3791/1266. PubMed PMID: 19574953;
480 PubMed Central PMCID: PMCPMC2798855.

481 35. Xin G, Chen Y, Topchyan P, Kasmani MY, Burns R, Volberding PJ, et al. Targeting
482 PIM1-Mediated Metabolism in Myeloid Suppressor Cells to Treat Cancer. *Cancer
483 Immunol Res*. 2021;9(4):454-69. Epub 2021/02/14. doi: 10.1158/2326-6066.CIR-20-
484 0433. PubMed PMID: 33579728; PubMed Central PMCID: PMCPMC8137571.

485

486
487

488 **FIGURE LEGENDS**

489

490 **FIGURE 1. Mtb-infected ACE2 mice are resistant to secondary infection with CoV2.**

491 (A) Experimental overview of our ACE2:CoV2 model studies, wherein mice were infected
492 via aerosol with Mtb (Day -30) and challenged 30 days later (Day 0) with CoV2. On post-
493 challenge Day 4, Day 7 and Day 14, tissues were collected for microbiological and
494 immunological assessments. Experimental groups included ACE2 mice which were not
495 infected with Mtb prior to CoV2 challenge ($Mtb^{NEG}CoV2^{POS}$), ACE2 mice which were
496 infected with Mtb but challenged with sterile saline ($Mtb^{POS}CoV2^{NEG}$), ACE2 mice which
497 were infected with Mtb prior to CoV2 challenge ($Mtb^{POS}CoV2^{POS}$), and B6 controls which
498 were infected with Mtb (to determine what if any impact human ACE2 transgene
499 expression alone has on Mtb burdens). (B) The percent weight change experienced by
500 each group of ACE2 mice following CoV2 challenge, as normalized to the original weight
501 of each mouse. (C) CoV2 PFU burdens and (D) CoV2 N protein levels in the lungs of
502 $Mtb^{NEG}CoV2^{POS}$ and $Mtb^{NEG}CoV2^{POS}$ mice. (E-G) Mtb CFU burdens in the (E) lungs, (F)
503 spleen and (G) liver of $Mtb^{POS}CoV2^{NEG}$ and $Mtb^{POS}CoV2^{POS}$ mice, as well as B6 controls
504 throughout the experiment time course. In each graph the following legend applies:
505 $Mtb^{NEG}CoV2^{POS}$, black circles or bars; $Mtb^{POS}CoV2^{NEG}$, gray circles; $Mtb^{POS}CoV2^{POS}$,
506 white circles or bars. (H) Representative micrographs of AFB stained lung sections, as
507 collected from $Mtb^{POS}CoV2^{NEG}$ and $Mtb^{POS}CoV2^{POS}$ mice at the indicated times post-
508 challenge. In each micrograph, the large scale bar is 20 μ M and inset scale bar is 5 μ m.
509 This experiment was repeated twice, each with similar results (4 mice/group/timepoint).
510 *, p \leq 0.05 as determined by either Student's t-test or ANOVA; n.s., not significant.

511

512 **FIGURE 2. CoV2-elicited cytokine responses are muted in the presence of Mtb**
513 **infection.** On the indicated days, lung tissue from $Mtb^{NEG}CoV2^{POS}$, $Mtb^{POS}CoV2^{NEG}$,
514 $Mtb^{POS}CoV2^{POS}$ and uninfected (UI) ACE2 mice was used to measure (A-C) protein levels
515 of (A) $IFN\gamma$, (B) IL6 and (C) IL1 β , as well as (D-I) mRNA levels of (D) $IFN\gamma$, (E) $TNF\alpha$, (F)
516 IFIT2, (G) IFIT3, (H) CCL2 and (I) IL10. This experiment was repeated twice, each with
517 similar results (4 mice/group/timepoint). *, p ≤ 0.05 as determined by either Student's t-
518 test or ANOVA; §, significant relative to UI protein levels.

519

520 **FIGURE 3. CoV2 infection of the airways and associated pneumonia are attenuated**
521 **in the presence of Mtb.** Representative micrographs of (A-B) H&E and (C-D) CoV2 N
522 protein IHC stained lung sections from each experimental group, as collected on (A, C)
523 Day 4 or (B, D) Day 7 post challenge. In each micrograph the large scale bar represents
524 200 microns; insets are 50 microns.

525

526 **FIGURE 4. Mtb-infected B6 mice are resistant to secondary infection with MACoV2.**
527 (A) Experimental overview of our B6:MACoV2 model studies, wherein mice were infected
528 via aerosol with Mtb (Day -30) and challenged 30 days later (Day 0) with MACoV2. On
529 post-challenge Days 4, 7 and 14 we collected lung tissue for microbiological and
530 immunological assessments. Experimental groups included B6 mice which were not
531 infected with Mtb prior to MACoV2 challenge ($Mtb^{NEG}MACoV2^{POS}$), B6 mice which were
532 infected with Mtb but challenged with sterile saline ($Mtb^{POS}MACoV2^{NEG}$), and B6 mice
533 which were infected with Mtb prior to CoV2 challenge ($Mtb^{POS}MACoV2^{POS}$). (B) The

534 percent weight change experienced by each group of B6 mice following MACoV2
535 challenge, as normalized to the original weight of each mouse. **(C-D)** Lung viral burdens
536 in $Mtb^{NEG}MACoV2^{POS}$ and $Mtb^{POS}MACoV2^{POS}$ mice, as measured by **(C)** MACoV2 PFU
537 or **(D)** MACoV2 N protein concentration on the indicated days, as well as **(E)** lung Mtb
538 CFU burdens at the same timepoints. **(F, H)** Lung protein levels of **(F)** $IFN\gamma$ and **(H)** $IL6$,
539 as well as **(G, I-K)** mRNA levels of **(G)** $IFN\gamma$, **(I)** $IFIT3$, **(J)** $IFITM3$ and **(K)** $ACE2$. This
540 experiment was repeated twice, each with similar results (4 mice/group/timepoint). *, p ≤
541 0.05 as determined by either Student's t-test or ANOVA; §, significant relative to UI protein
542 levels.

543

544 **FIGURE 5. Lung T and B cell subsets expand upon challenge of Mtb^{POS} mice with**
545 **MACoV2.** As an unbiased means to define and compare the lung immune landscape,
546 live CD45+ cells were purified from the lungs of four experimental groups (Uninfected, UI;
547 $Mtb^{NEG}MACoV2^{POS}$; $Mtb^{POS}MACoV2^{NEG}$; $Mtb^{POS}MACoV2^{POS}$) on post-challenge Day 7
548 and used for scRNA analysis. **(A-C)** t-SNE plots of the resulting data, either **(A-B)** pooled
549 across groups or **(C)** segregated by group to show **(A)** the extent of overlay and **(B-C)**
550 clustering of data into 12 immune lineages. **(D)** The distribution and expression patterns
551 of lineage defining genes which we used to annotate each cluster, as pooled from all
552 group data (individual group data are shown in **Supplemental Figure 1**). **(E)** The
553 proportion of each immune lineage in the lungs of each experimental group. MØ,
554 macrophage; DC, dendritic cell; NK, natural killer.

555

556 **SUPPLEMENTAL FIGURE 1. Lineage defining markers were similarly expressed**
557 **across uninfected (UI), $Mtb^{NEG}MACoV2^{POS}$, $Mtb^{POS}MACoV2^{NEG}$ and**
558 **$Mtb^{POS}MACoV2^{POS}$ groups.** The distribution and expression patterns of lineage defining
559 genes that were used to annotate each t-SNE cluster, as shown for each individual
560 experimental group (pooled group data are shown in **Figure 5**).

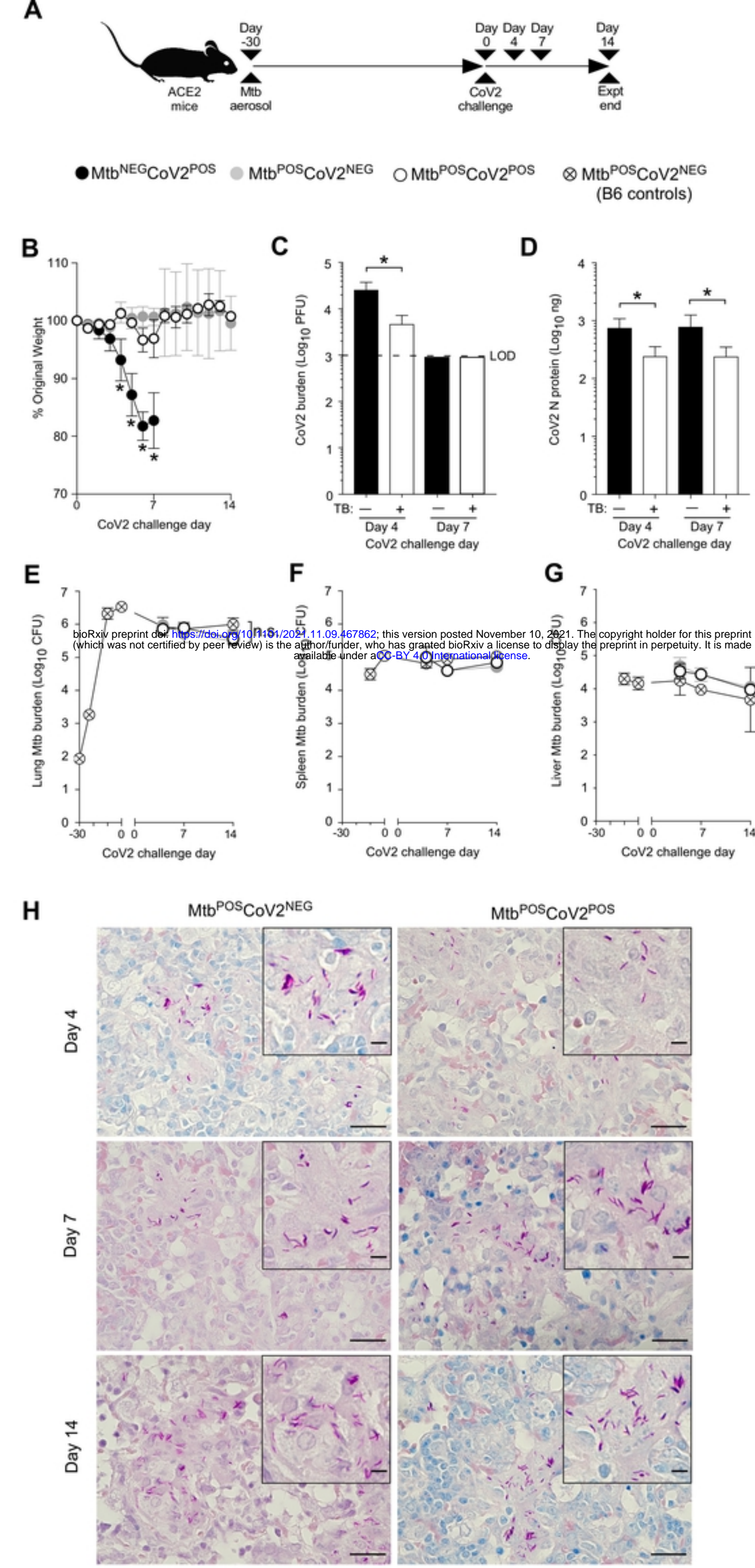


FIG 1

Figure 1

● Uninfected (UI) ● Mtb^{NEG}CoV2^{POS} ● Mtb^{POS}CoV2^{NEG} ○ Mtb^{POS}CoV2^{POS}

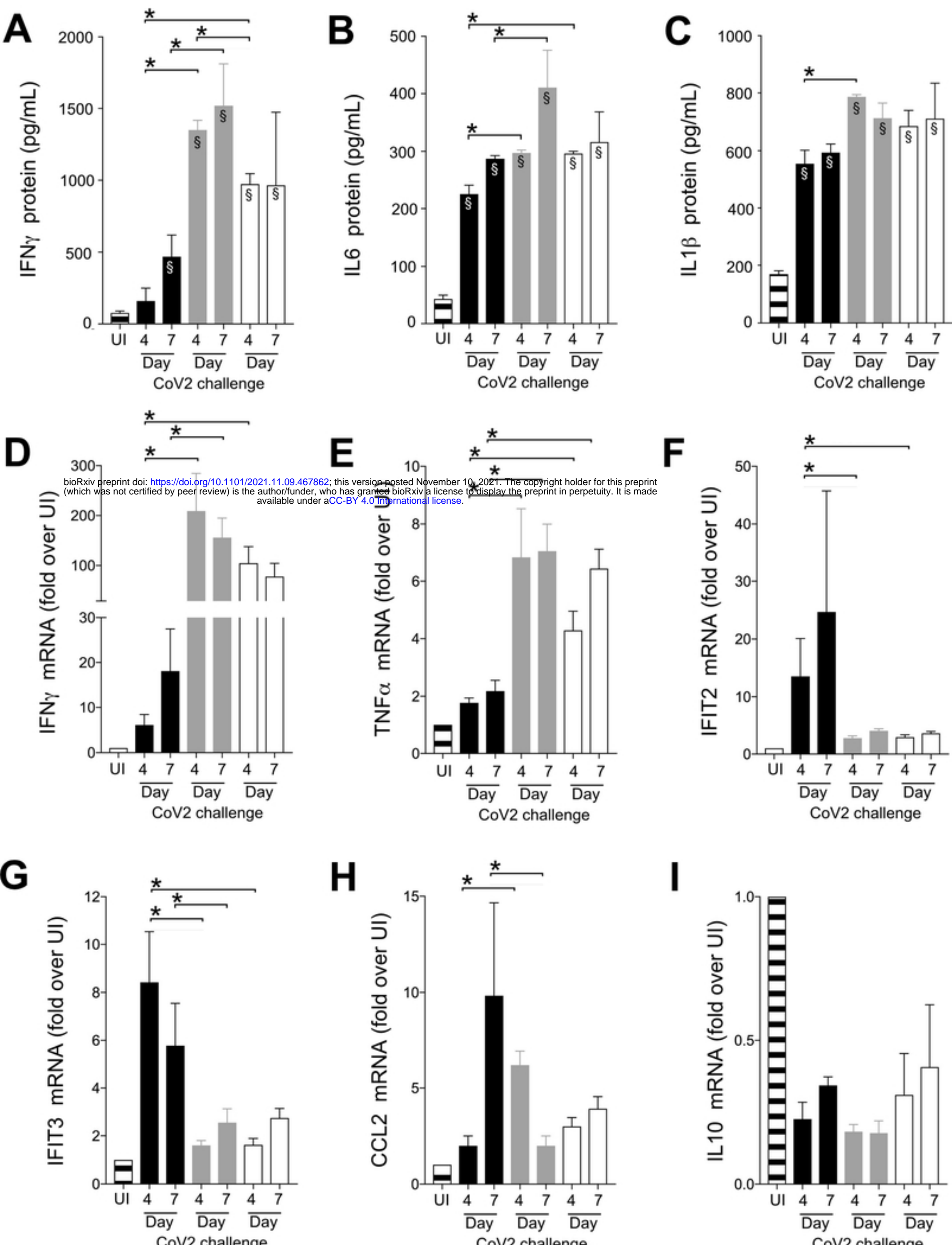


FIG 2

Figure 2

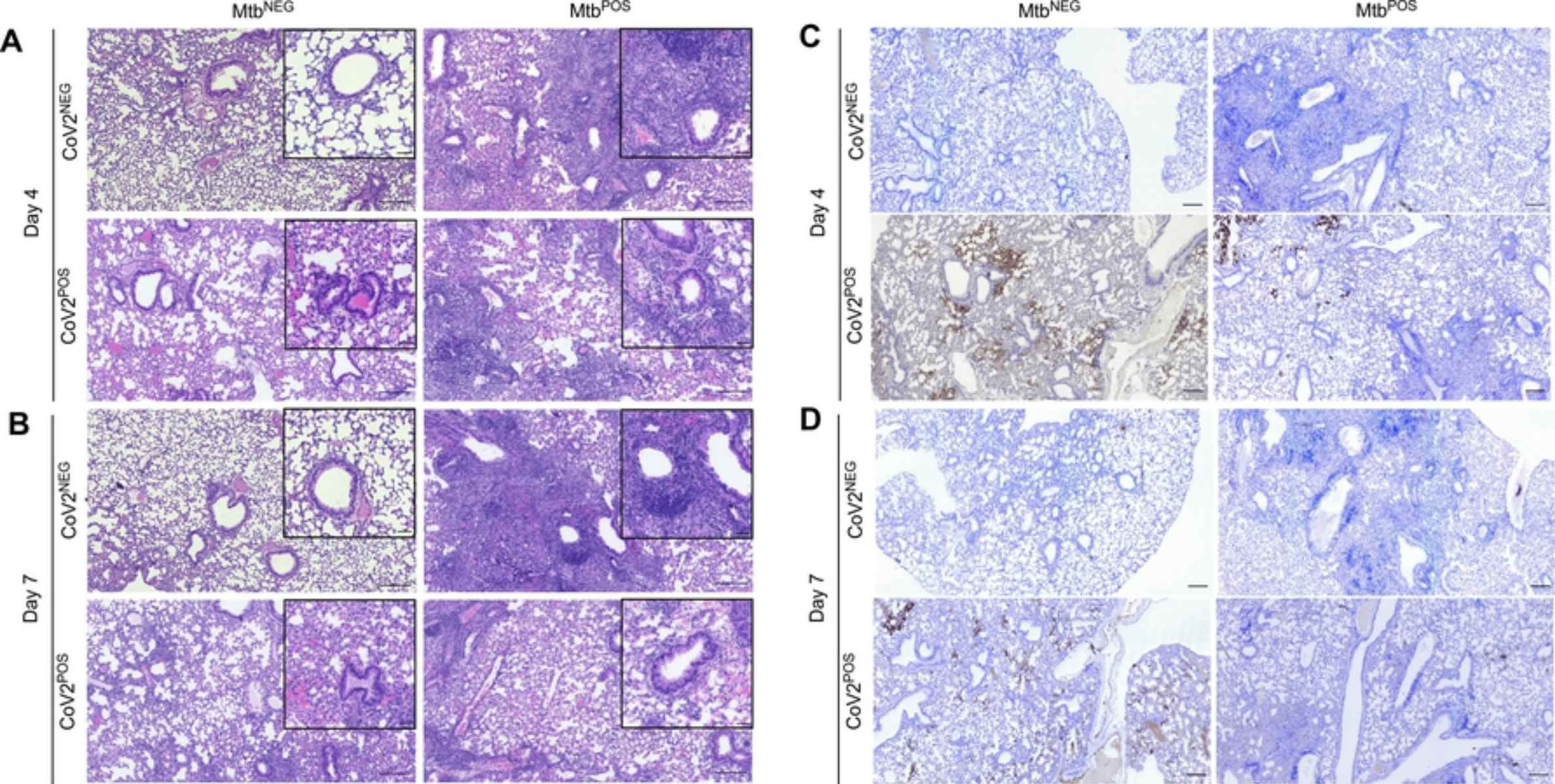


Figure 3

FIG 3

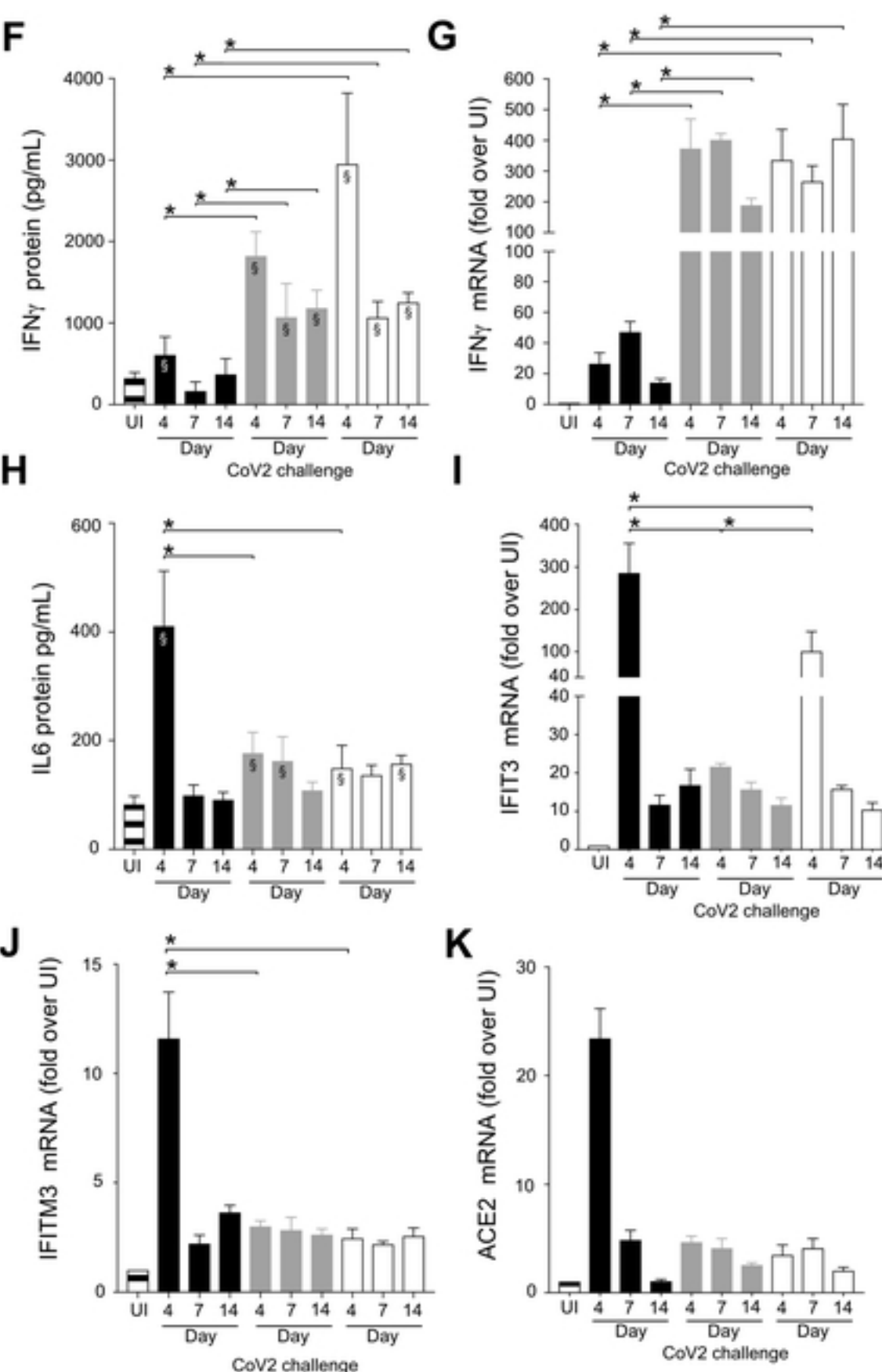
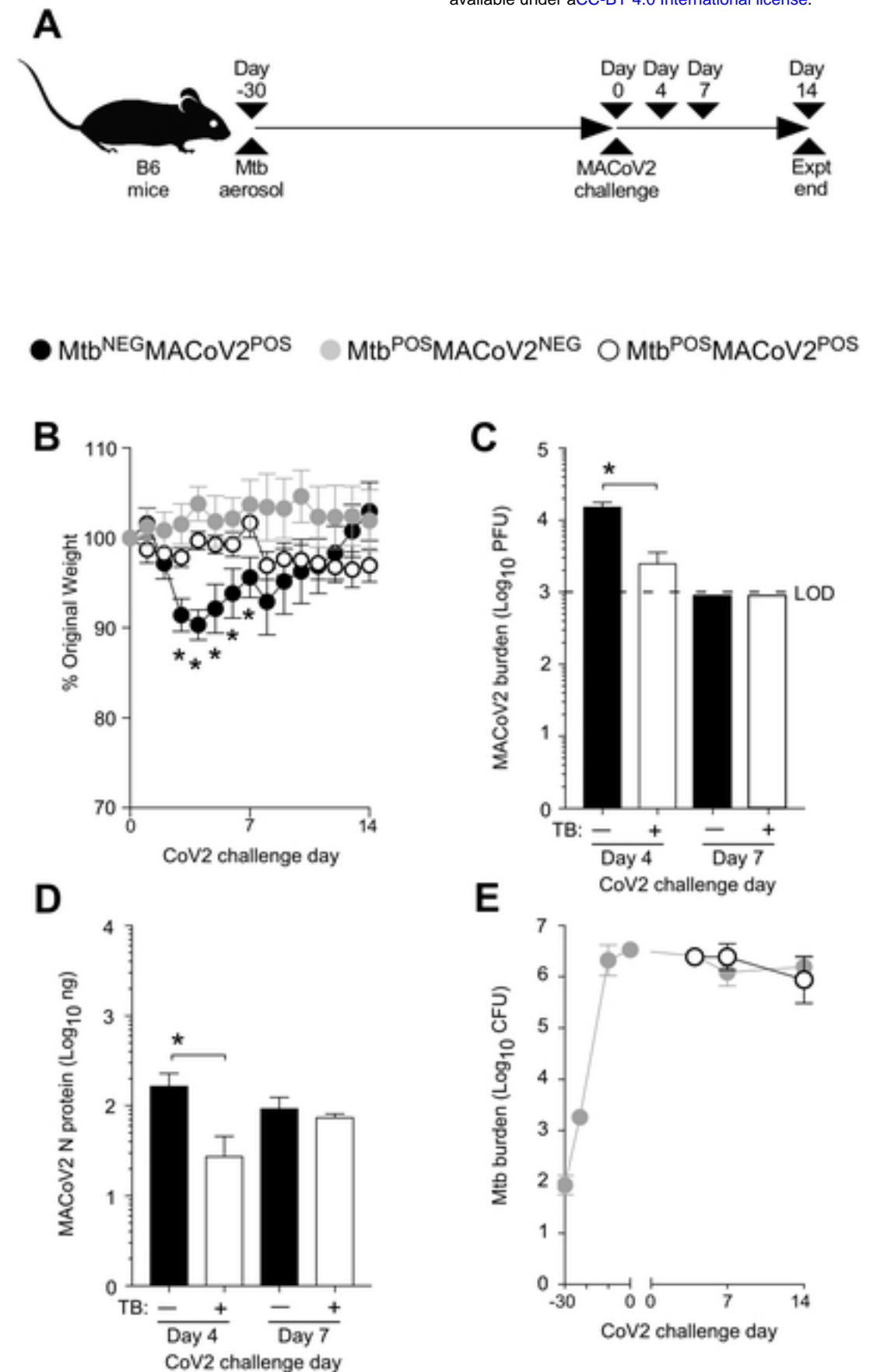


Figure 4

FIG 4

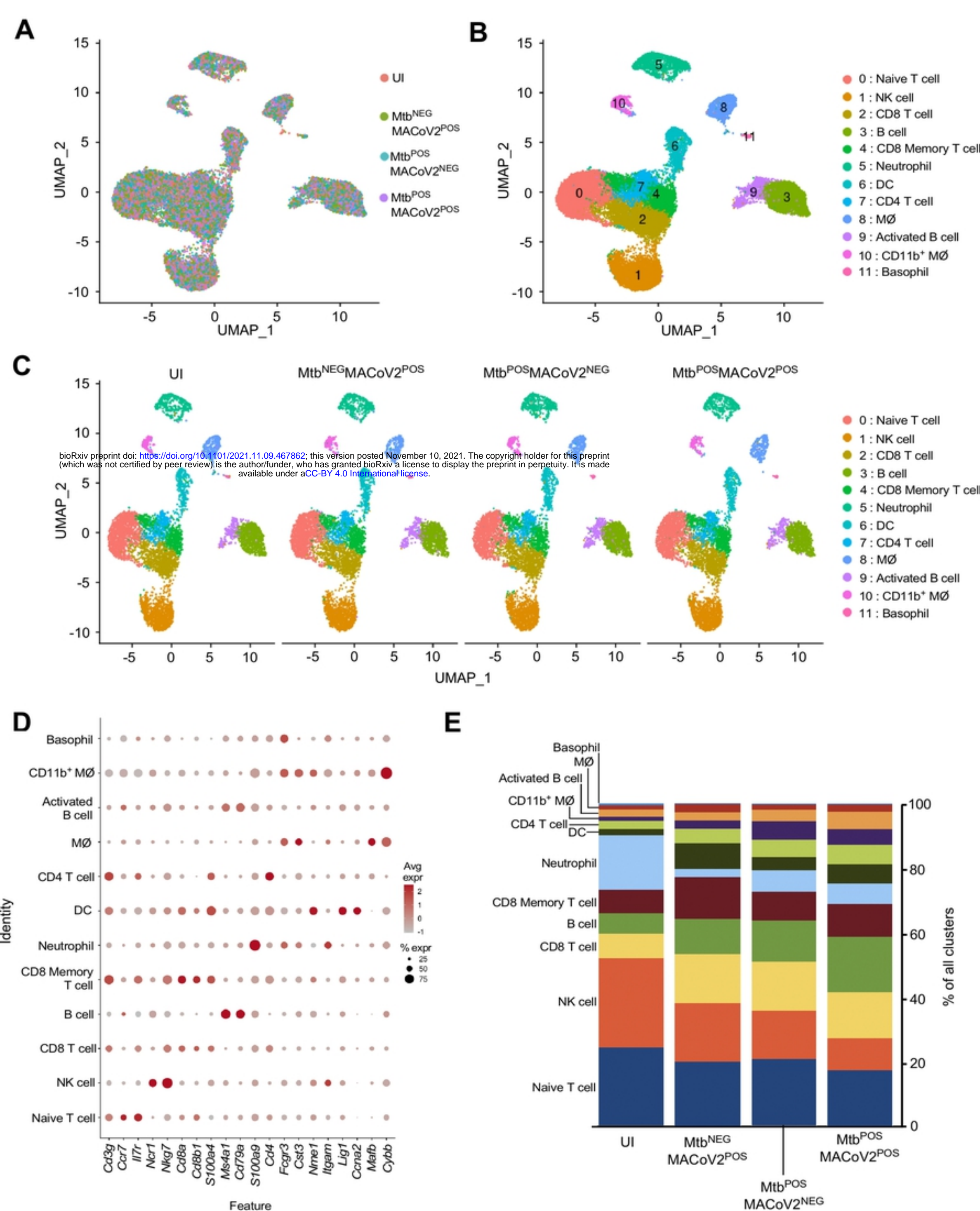


Figure 5

FIG 5